

RESEARCH

Open Access



# Genetic alterations that deregulate RB and PDGFRA signaling pathways drive tumor progression in *IDH2*-mutant astrocytoma

Kensuke Tateishi<sup>1,2,3\*</sup> , Yohei Miyake<sup>1,3</sup>, Taishi Nakamura<sup>1,3</sup>, Hiromichi Iwashita<sup>4,5</sup>, Takahiro Hayashi<sup>1,3</sup>, Akito Oshima<sup>1,3</sup>, Hirokuni Honma<sup>1,3</sup>, Hiroaki Hayashi<sup>3,6</sup>, Kyoka Sugino<sup>1,2,3</sup>, Miyui Kato<sup>2,3</sup>, Kaishi Satomi<sup>7</sup>, Satoshi Fujii<sup>5,8</sup>, Takashi Komori<sup>9</sup>, Tetsuya Yamamoto<sup>1</sup>, Daniel P. Cahill<sup>10,11</sup> and Hiroaki Wakimoto<sup>10,11</sup>

## Abstract

In *IDH*-mutant astrocytoma, *IDH2* mutation is quite rare and biological mechanisms underlying tumor progression in *IDH2*-mutant astrocytoma remain elusive. Here, we report a unique case of *IDH2* mutant astrocytoma, CNS WHO grade 3 that developed tumor progression. We performed a comprehensive genomic and epigenomic analysis for primary and recurrent tumors and found that both tumors harbored recurrent *IDH2*<sup>R172K</sup> and *TP53*<sup>R248W</sup> mutation with *CDKN2A/B* hemizygous deletion. We also found amplifications of *CDK4* and *MDM2* with *PDGFRA* gain in the recurrent tumor and upregulated protein expressions of these genes. We further developed, for the first time, a xenograft mouse model of *IDH2*<sup>R172K</sup> and *TP53*<sup>R248W</sup> mutant astrocytoma from the recurrent tumor, but not from the primary tumor. Consistent with parent recurrent tumor cells, amplifications of *CDK4* and *MDM2* and *PDGFRA* gain were found, while *CDKN2A/B* was identified as homozygous deletion in the xenografts, qualifying for integrated diagnosis of astrocytoma, *IDH2*-mutant, CNS WHO grade 4. Cell viability assay found that CDK4/6 inhibitor and PDGFR inhibitor potentially decreased cell viability in recurrent tumor cells, as compared to primary tumor cells. These findings suggest that gene alterations that activate retinoblastoma (RB) signaling pathways and PDGFR may drive tumor progression and xenograft formation in *IDH2*-mutant astrocytoma, which is equivalent to progressive *IDH1*-mutant astrocytoma. Also, our findings suggest that these genomic alterations may represent therapeutic targets in *IDH2*-mutant astrocytoma.

**Keywords** *IDH2* mutation, Astrocytoma, Malignant phenotype, PDX

\*Correspondence:

Kensuke Tateishi  
kate12@yokohama-cu.ac.jp

<sup>1</sup> Department of Neurosurgery, Graduate School of Medicine, Yokohama City University, 3-9 Fukuura, Kanazawa, Yokohama 2360004, Japan

<sup>2</sup> Laboratory of Biopharmaceutical and Regenerative Science, Graduate School of Medical Science, Yokohama City University, Yokohama, Japan

<sup>3</sup> Neurosurgical-Oncology Laboratory, Yokohama City University, Yokohama, Japan

<sup>4</sup> Department of Pathology, Yokohama City University Hospital, Yokohama, Japan

<sup>5</sup> Department of Diagnostic Pathology, Yokohama City University Hospital, Yokohama, Japan

<sup>6</sup> Department of Pediatrics, Graduate School of Medicine, Yokohama City University, Yokohama, Japan

<sup>7</sup> Department of Pathology, Kyorin University School of Medicine, Tokyo, Japan

<sup>8</sup> Department of Molecular Pathology, Graduate School of Medicine, Yokohama City University, Yokohama, Japan

<sup>9</sup> Department of Laboratory Medicine and Pathology (Neuropathology), Tokyo Metropolitan Neurological Hospital, Tokyo, Japan

<sup>10</sup> Department of Neurosurgery, Massachusetts General Hospital, Boston, MA, USA

<sup>11</sup> Translational-Neurooncology Laboratory, Brain Tumor Research Center, Massachusetts General Hospital/Harvard Medical School, Boston, MA, USA



© The Author(s) 2023. **Open Access** This article is licensed under a Creative Commons Attribution 4.0 International License, which permits use, sharing, adaptation, distribution and reproduction in any medium or format, as long as you give appropriate credit to the original author(s) and the source, provide a link to the Creative Commons licence, and indicate if changes were made. The images or other third party material in this article are included in the article's Creative Commons licence, unless indicated otherwise in a credit line to the material. If material is not included in the article's Creative Commons licence and your intended use is not permitted by statutory regulation or exceeds the permitted use, you will need to obtain permission directly from the copyright holder. To view a copy of this licence, visit <http://creativecommons.org/licenses/by/4.0/>. The Creative Commons Public Domain Dedication waiver (<http://creativecommons.org/publicdomain/zero/1.0/>) applies to the data made available in this article, unless otherwise stated in a credit line to the data.

## Introduction

Since the discovery of *IDH1* mutation in gliomas [30], *IDH1* mutation has been considered one of the most fundamental genetic alterations in diffuse lower-grade gliomas (LGGs). In *IDH*-mutant gliomas, the vast majority of mutations are at codon 132 of *IDH1* and mostly heterozygous substitution from arginine to histidine (R132H) [35, 46]. Astrocytoma typically harbors *IDH1*, *TP53*, and *ATRX* mutations [4, 20]. In general, *IDH1*-mutant astrocytomas have better prognosis than *IDH1/2*-wildtype gliomas. However, most *IDH1*-mutant astrocytomas eventually develop a malignant phenotype [25]. Several studies have uncovered molecular mechanisms of malignant transformation in *IDH1*-mutant astrocytoma [5, 33, 37, 42]. For instance, we have demonstrated that additional “tertiary mutations”, such as *PDGFRA* and *MYCN* amplification, promoted patient tumor progression and xenograft formation in *IDH1*-mutant astrocytoma. We also found that xenograft formation was correlated with poor prognosis in *IDH1*-mutant astrocytoma patients [42]. Using genetically engineered mouse models, Philip et al. reported that *IDH1*<sup>R132H</sup> cooperated with *PDGFA* and loss of *Cdkn2a*, *Atrx*, and *Pten* to promote high-grade astrocytoma in vivo [31]. These data indicate that acquired pathogenic gene alterations promote tumor progression in *IDH1*-mutant astrocytoma, resulting in dismal outcomes.

In mammalian cells, *IDH1* is located in the cytoplasm, while *IDH2* is in the mitochondria. *IDH2* mutation is commonly found in acute myeloid leukemia [45]. On the other hand, *IDH2*<sup>R172</sup> mutation was also identified in astrocytoma, with less than 3% frequency [9]. Another study analyzed 811 glioma samples and identified only 3 of 266 (1.1%) astrocytomas harbored *IDH2*-mutation [44]. These findings suggest that *IDH2*-mutation is quite rare in astrocytoma. Both mutant *IDH1* and *IDH2* inhibit this enzymatic activity and instead produce 2-hydroxyglutarate (2-HG) from  $\alpha$ -KG. 2-HG induces the global DNA and histone methylation phenotype by blocking  $\alpha$ -KG dependent dioxygenases and promote gliomagenesis [12, 14, 29]. Therefore, *IDH2* mutation is considered as equivalent to *IDH1* mutation and *IDH2*-mutant gliomas are conventionally analyzed along with *IDH1*-mutant gliomas. However, the molecular mechanisms of malignant progression are poorly understood in *IDH2*-mutant astrocytoma. Additionally, since *IDH2*-mutant glioma xenograft model is lacking, translational insight is scant to date. Here, we report a patient with *IDH2*<sup>R172K</sup>-mutant astrocytoma that progressed during follow-up. We comprehensively performed genomic and epigenomic analyses for both the initial and recurrent tumors. We further developed the first *IDH2*<sup>R172K</sup> mutant astrocytoma, CNS WHO grade 4 xenograft mouse model from recurrent

tumor. Our data reveal a molecular mechanism of how genomic alterations promote tumor progression and xenograft formation in *IDH2*-mutant astrocytoma.

## Material and methods

### Creation of primary cultured cells

Fresh tumor specimens were obtained from surgery and enzymatically dissociated with 0.1% of Trypsin and DNase. Primary cultured cells were maintained in serum-free neural stem cell medium (Neurobasal Medium, Gibco), supplemented with L-glutamine (Gibco), B27 (Gibco), N2 (Gibco), human recombinant EGF (R&D Systems), human FGF-basic (Alomone Labs), and Antibiotic–Antimycotic (Gibco) as previously described [41]. Dissociated cells were cryopreserved and used for in vitro experiments.

### Cell viability analysis

To assess cell viability, tumor cells were dissociated into single cells and seeded into 96-well plates at 3000 cells/well. After 6 h, chemical inhibitors were serially diluted and added to wells. Cell viability was measured by CellTiter-Glo (Promega) assay at day 3. The relative cell viability was indicated as the percentage viability of the DMSO control. Abemaciclib (Selleck), AC710 (Tocris Bioscience), Enasidenib (AG-221, MedChemExpress), GDC-0068 (Cayman), LY294002 (Selleck), Palbociclib (Toronto Research chemicals), and Tyrphostin A9 (Focus Biomolecules) were used.

### Xenograft models

$1 \times 10^5$  Cells were orthotopically implanted into the right striatum of 4–6 week-old female SCID Beige mice (Charles River, Yokohama) within 12 h after dissociation. Mice were monitored 2–3 times per week and sacrificed when neurologic deficits or general conditions reached the criteria for euthanasia. Brains were harvested and used for pathological and genomic evaluation. All mouse experiments were approved by the Institutional Animal Care and Use Committee at YCU (IRB No. FA22-011).

### Western blotting

Cells were lysed in RIPA buffer (Sigma-Aldrich) with protease inhibitor cocktail tablets (Roche). Fifty  $\mu$ g of protein was separated by 10% SDS-PAGE and transferred to polyvinylidene difluoride membranes (Millipore) by electroblotting. After blocking with Bullet Blocking One for western blotting (Nacalai Tesque), the membranes were incubated with primary antibodies at 4 °C overnight. After washing and incubation with horseradish peroxidase–conjugated secondary antibodies (CST), the blots were washed, and the signals were visualized with chemiluminescent HRP substrate (Merck Millipore). The

primary antibodies used were cleaved-PARP ([diluted 1:1000], GeneTex, Cat. #GTX132329), GAPDH ([diluted 1:4000], GeneTex, Cat. #GTX100118), IDH2<sup>R172K</sup> ([diluted 1:500], Medical and Biological laboratories, MBL, Cat. #D328-3), H3K27me3 ([diluted 1:5000], Cell Signaling Technology, CST, Cat. #9733 T), H3K9me3 ([diluted 1:5000], Abcam, Cat. #ab8898), Histone H3 antibody ([diluted 1:5000], Abcam, Cat. #ab1791), phospho-AKT ([diluted 1:1000], GeneTex, Cat. #GTX128414), phospho-ERK ([diluted 1:1000], Bethyl Laboratories, Cat. #A303-608A-M), phospho-MEK ([diluted 1:1000], CST, Cat. #9154S), and phospho-mTOR ([diluted 1:500], Merck, Cat. #09-213). Western blotting images were evaluated qualitatively.

### Histopathological analysis

Tumor tissue specimens were fixed in 10% neutral-buffered formalin and embedded in paraffin. Hematoxylin and eosin staining was performed using standard procedures. For immunohistochemistry, 5- $\mu$ m thick sections were deparaffinized, treated with 0.5% H<sub>2</sub>O<sub>2</sub> in methanol, rehydrated, and heated in a microwave for 20 min for antigen retrieval. After blocking with serum, tissue sections were incubated with primary antibodies against Akt ([diluted 1:1000], CST, Cat. #4691), CDK4 ([diluted 1:1000], Bioss Antibodies, Cat. #BS-0633R), ERK ([diluted 1:1000], CST, Cat. #4695), Ki-67 ([diluted 1:1000], Novus Biologicals, Cat. #NB600-1252), MDM2 ([diluted 1:1000], GeneTex, Cat. #GTX100531), p53 ([diluted 1:1000], Novus Biologicals, Cat. #NBP2-44982), phospho-AKT ([diluted 1:1000], GeneTex, Cat. #GTX128414), phospho-ERK ([diluted 1:1000], Bethyl Laboratories, Cat. #A303-608A), phospho-PDGFR $\alpha$  ([diluted 1:1000], CST, Cat. #3170 T), and phospho-Rb ([diluted 1:1000], CST, Cat. #8516S) at 4 °C overnight. The next day, the sections were washed with phosphate-buffered saline, incubated with biotinylated secondary antibodies for 30 min at room temperature, and then incubated with ABC solution (PK-6101, PK-6102; Vector Laboratories) for 30 min. Finally, the sections were incubated with DAB (K3467, Dako) and counterstained with hematoxylin. Three images per each specimen were obtained for quantitative analysis. Cells positive for phosphorylated proteins were evaluated quantitatively. Only strongly stained cells were considered positive.

### Genomic analysis

Genomic DNA was extracted using Dneasy Blood & Tissue (Qiagen), according to the manufacturer's protocol. To evaluate single nucleotide variants (SNVs), insertion/deletion, and copy number alterations (CNAs), whole exome sequencing (WES) was performed as previously described [38]. Somatic SNV was detected by MuTect,

while the somatic InDel was identified by Strelka. Control-FREEC was used to detect somatic CNV. ANNOVAR was used to perform variant annotation. dbSNP, COSMIC, OMIM, GWAS Catalog, and HGMD were used to find reported information of the variants [23]. The multiplex polymerase chain reaction (PCR) technology (MGH SNaPshot) was also performed for validation, as previously described [39]. IDH1<sup>R132H</sup> and IDH2<sup>R172K</sup>, TP53<sup>R248W</sup>, and TERT promoter SNVs were also assessed by Sanger sequencing. Primer sequences for Sanger sequencing are listed in the Additional file 2: Table S1. CDK4, CDKN2A, EGFR, MDM2, PDGFRA, PTEN, and TP53 CNAs were selectively assessed using multiplex ligation-dependent probe amplification (MLPA), according to the manufacturer's instructions (SALSA MLPA KIT probe mix P105-D3, MRC-Holland). SALSA MLPA KIT probe mix P088-C2 was used to validate chromosome 1p and/19q and CDKN2A status. The MLPA data were collected using an ABI 3730xL Genetic Analyzer (FASMAC, Japan) and analyzed using Coffalyzer.Net Software (MRC-Holland). The copy number status was defined using the following thresholds: homozygous deletion (HD,  $x < 0.4$ ), hemizygous deletion ( $0.4 < x < 0.7$ ), gain ( $1.3 < x < 2.0$ ), and amplification ( $x > 2.0$ ), according to previous studies [17].

### DNA methylation array analysis

The Infinium MethylationEPIC v.1.0 BeadChip Kit (Illumina) was used to obtain genome-wide DNA methylation profiles and copy number alterations. The detailed protocol has been described previously [16]. The cut-off value for amplification (0.35) and homozygous deletion ( $-0.415$ ) was used [37].

### Statistical analysis

Statistical analysis was performed using JMP Pro17.0.0 software (Cary, NC) and GraphPad Prism (ver. 10.0.3, San Diego, CA). For parametric analysis, a two-tailed *t*-tests was used. Survival analysis using datasets was performed by Kaplan–Meier method, and the log-rank test was used to compare survival differences. The data were expressed as the mean  $\pm$  SEM. *P*-value  $< 0.05$  was considered as statistically significant.

## Results

### Case presentation

A 44-year-old man complained a headache. Magnetic resonance imaging (MRI) demonstrated a non-enhancing tumor with surrounding edema in the right frontal lobe. The T2/FLAIR mismatch sign was observed (Fig. 1A, upper panels). <sup>18</sup>F-fluorodeoxyglucose (FDG)-PET demonstrated a lower uptake in the tumor, compared with the contralateral cerebral hemisphere. <sup>11</sup>C-methionine

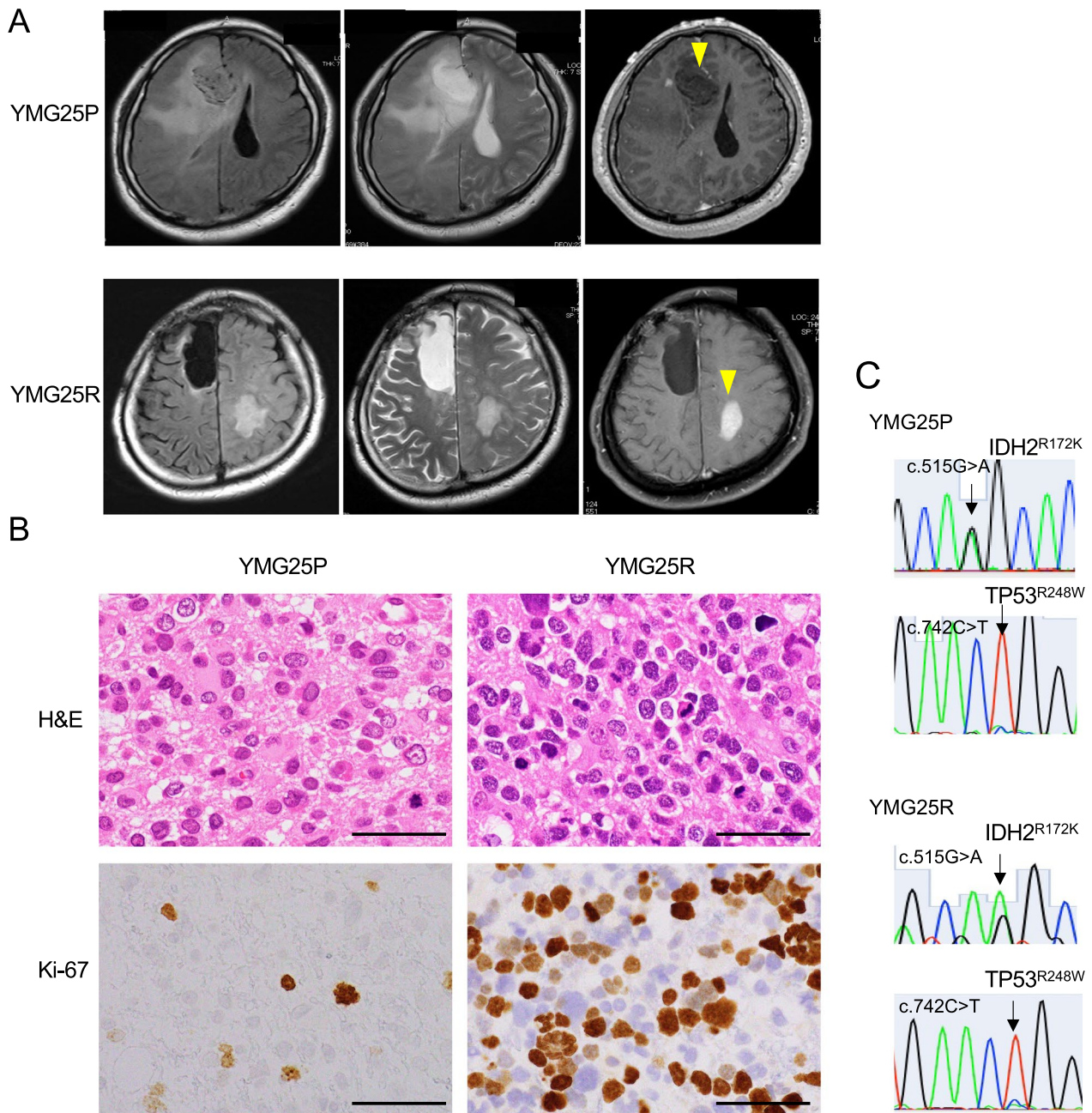


**Fig. 1** Clinical characteristics of *IDH2*-mutant astrocytoma patient. **A** Magnetic resonance imaging showing FLAIR (left), T2-weighted (middle), and gadolinium-enhanced T1-weighted (right) images for initial tumor (YMG25P, upper panel) and recurrent tumor (YMG25R, lower panel). **B** Hematoxylin and eosin staining (upper) and Ki-67 immunohistochemistry (lower) for YMG25P (left) and YMG25R (right) tumors. Bars, 50  $\mu$ m. **C** Sanger sequencing indicating *IDH2* (c.515G>A, R172K) and *TP53* (c.742C>T, R248W) mutation in YMG25P (upper) and YMG25R (lower)

(MET)-PET revealed a weak uptake of the tumor (maximum standardized uptake value; 2.0, Additional file 1: Fig. S1A). We performed subtotal tumor resection at the right superior frontal gyrus (YMG25P). Hematoxylin and eosin staining showed high cellular proliferation of astrocytic cells with 4 mitotic figures per  $\text{mm}^2$ . Nuclear

atypia was observed, while microvascular proliferation and necrosis were absent (Fig. 1B). Immunostaining for p53 was positive, whereas *IDH1*<sup>R132H</sup> was negative and *ATRX* was lost (Additional file 1: Fig. S1B). Pathogenic mutations of *IDH2*<sup>R172K</sup> and *TP53*<sup>R248W</sup> were identified, (Fig. 1C, Additional file 2: Tables S2 and S3). On the

other hand, *ATRX* and *TERT* promoter SNV were not identified.

Postoperatively, the patient received radiotherapy (60 Gy/30 fractions) with concomitant temozolomide (TMZ), and was subsequently treated with TMZ for 24 cycles. However, 32 months after the initial diagnosis, MRI demonstrated a contrast enhancing tumor in the contralateral left parietal lobe (Fig. 1A, lower panels). T2/FLAIR imaging showed a high signal intensity mass lesion, which was discontinuous from the initial tumor. We performed gross total resection of this tumor (YMG25R). Hematoxylin and eosin staining demonstrated high cellularity with 20 mitotic figures per mm<sup>2</sup> in the recurrent tumor, but necrosis and microvascular proliferation were scant. The Ki-67 labeling index was 26% in YMG25R, which was relatively higher than that of YMG25P (11%, Fig. 1B). Immunostaining for p53 was positive, whereas *IDH1*<sup>R132H</sup> was negative and *ATRX* was lost in YMG25R (Additional file 1: Fig. S1B), consistent with YMG25P. Genomic sequencing revealed the same *IDH2*<sup>R172K</sup> and *TP53*<sup>R248W</sup> heterozygous mutations (Fig. 1C). An elevated tumor mutation burden was found (23 mutations/Mb) in YMG25R, but additional pathogenic mutation was not identified (Additional file 2: Tables S2 and S3). After the second surgery, the patient received chemotherapy with procarbazine, nimustine, and vincristine. However, MRI showed progressive disease and bevacizumab was additionally administered. Forty-eight months after initial diagnosis, the patient passed away due to tumor progression.

Genome-wide DNA methylation array and MLPA revealed *CDKN2A* hemizygous deletion in YMG25R that was unchanged from YMG25P (Fig. 2A, Additional file 1: Fig. S2A). Also, partial deletion of chromosome 19 was found in YMG25P, while chromosome 1p and 19q partial deletion was observed in YMG25R (Fig. 2A, Additional file 1: Fig. S2B), which was described previously [28]. In YMG25P and YMG25R, methylation classifier results (version 11b4) indicated a classification matched to diffuse glioma, IDH mutant (Additional file 2: Table S4). Unsupervised clustering using t-SNE analysis, as indicated by DNA methylation analysis, demonstrated that both tumors were plotted close to astrocytoma, IDH-mutant (Fig. 2B). Methylation classifier (11b4) indicated subclass astrocytoma in YMG25P (score 0.63), and subclass high-grade astrocytoma in YMG25R (score 0.65, Fig. 2B, Additional file 2: Table S4). On the other hand, the newest version 12.8 matched YMG25P as diffuse glioma, IDH mutant and 1p/19q co-deleted in YMG25P (score 0.91), but did not match YMG25R to any classification (Additional file 2: Table S5). Since chromosome 1p/19q co-deletion, one of the essential criteria of “oligodendroglioma, IDH-mutant and 1p/19q-codeleted”,

was absent in both tumors, the results of the Classifier version 12.8 were discordant with the molecular diagnosis. Collectively, the integrated diagnosis of YMG25P and YMG25R was astrocytoma, IDH-mutant, CNS WHO grade 3. *MGMT* promoter was methylated in both tumors (*MGMT*-STP27, Additional file 1: Fig. S2C). The reason for the discordance between the results of version 11b4 and 12.8 is unknown and has not been provided on the DKFZ website.

Notably, amplifications of *CDK4* and *MDM2* and gain of *PDGFRA*, together with chromosome 4p gain were identified as newly acquired CNAs in YMG25R, as compared to the initial tumor YMG25P (Fig. 2A, Additional file 1: Fig. S2A). To assess differences of signaling pathway activation, we performed immunohistochemistry and western blot for phospho-PDGFR, -AKT, -mTOR, -MEK, and -ERK, comparing YMG25P and YMG25R in tissue and cells derived. We found that the expression levels of these phospho-proteins were higher in YMG25R compared to YMG25P (Fig. 3A-B, Additional file 1: Fig. S3A-B). We also found that *CDK4*, *MDM2*, and phospho-Rb were upregulated in YMG25R as compared to YMG25P (Fig. 3A, Additional file 1: Fig. 3A).

We established patient-derived cultures from YMG25P and YMG25R, and tested response to targeted agents. Interestingly, we found a significantly increased sensitivity to PDGFR inhibitors (Tyrphostin A9 and AC710) in YMG25R cells compared with YMG25P cells (Fig. 3C). No difference was observed in response to treatment with PI3K inhibitor (LY294002) and AKT inhibitor (GDC-0068, Additional file 1: Fig. S3C). We also found that *CDK4/6* inhibitors (Abemaciclib and Palbociclib) significantly decreased cell viability in YMG25R cells as compared with YMG25P cells (Fig. 3D). Previous clinical and preclinical studies have demonstrated that AML cells with *IDH2* mutation were highly sensitive to mutant *IDH2* specific inhibitors [13, 43, 48]. To examine the potential impact of mutant *IDH2* specific inhibitor on our *IDH2* mutant glioma cells, we performed cell viability assay and western blots. However, we did not find decreased cell viability or histone change in *IDH2* inhibitor (AG-221)-treated YMG25R cells (Additional file 1: Fig. S3D–F).

To assess the potential of xenograft formation, we attempted to establish orthotopic patient-derived xenograft models. YMG25P and YMG25R cells (1×10<sup>5</sup> cells) were stereotactically injected into SCID-Beige mouse brains. Of note, we observed reproducible xenograft formation in YMG25R-implanted mice, but not in YMG25P-implanted mice (Fig. 4A, B). Hematoxylin and eosin staining of YMG25R xenografts showed proliferative tumor cells with nuclear atypia (Fig. 4A). Immunohistochemical analysis demonstrated expression of p53

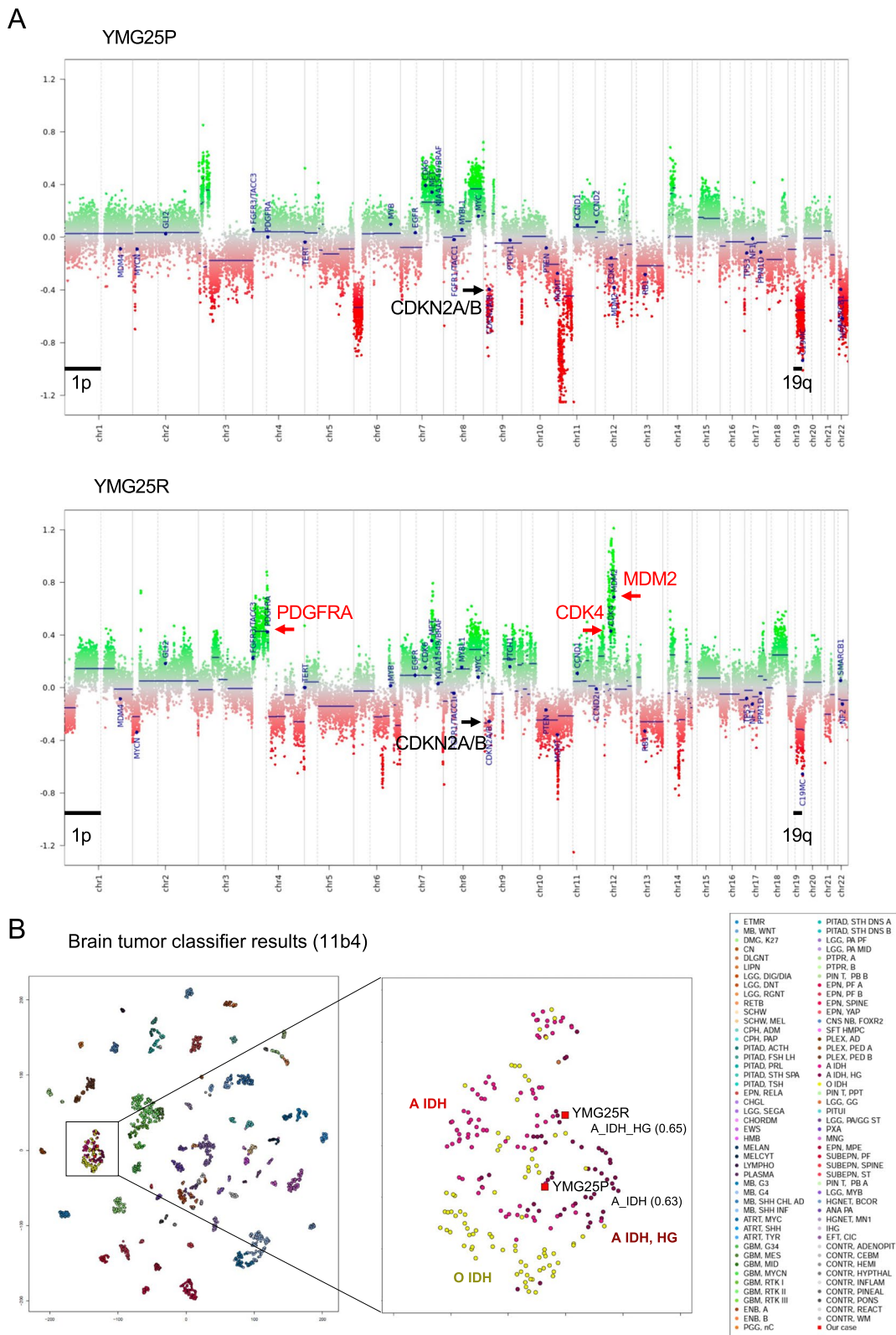


**Fig. 2** DNA methylation array-based tumor characteristics. **A** Copy number profiling of YMG25P (upper) and YMG25R (lower) tumor. **B** Unsupervised clustering using t-SNE analysis for initial tumor (YMG25P) and recurrent tumor (YMG25R). Brain tumor classifier was determined by version 11b4

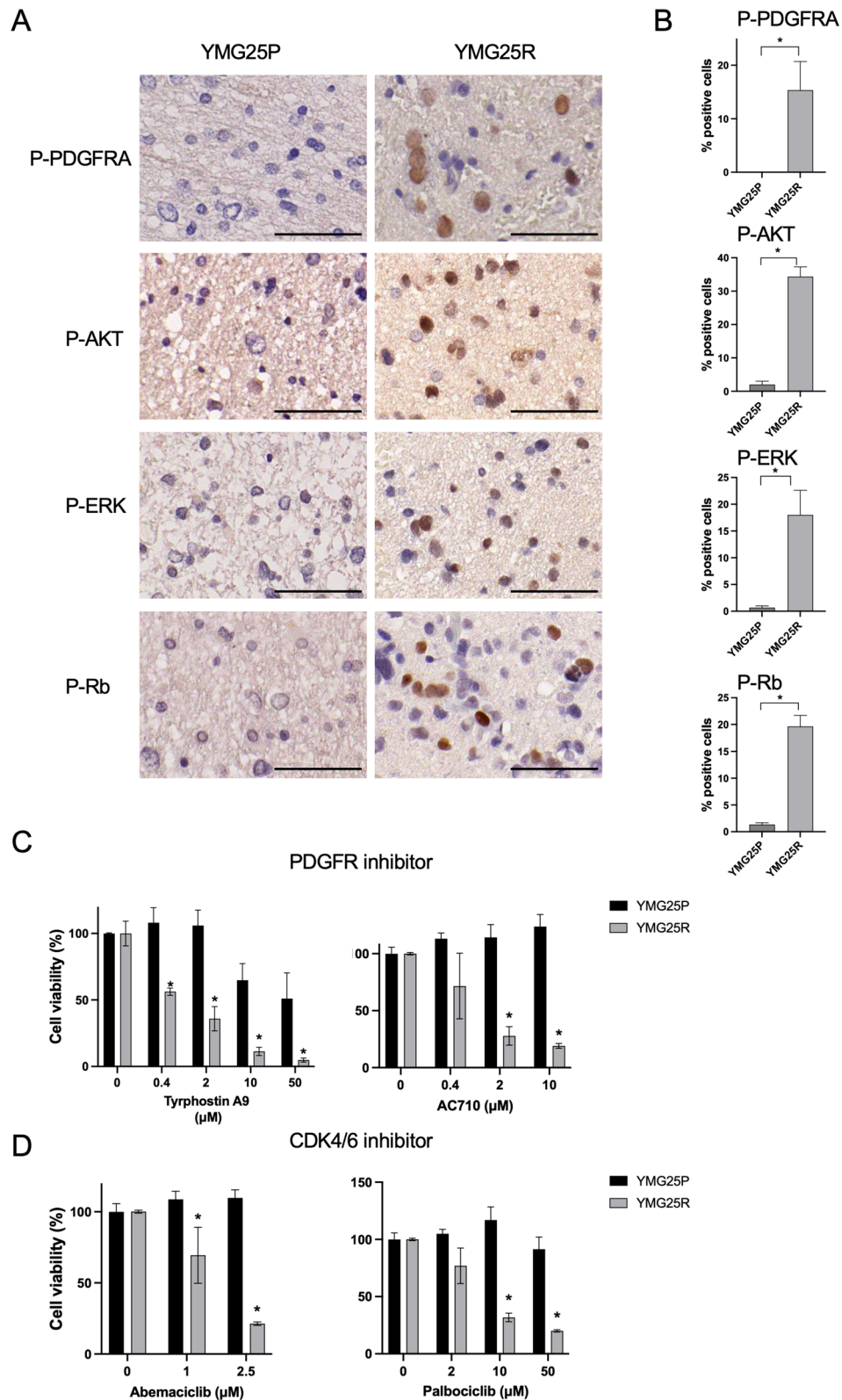


**Fig. 3** Protein expression and drug sensitivity for associated protein inhibitors. **A** Immunohistochemistry of indicated proteins for initial tumor (YMG25P, left) and recurrent tumor (YMG25R, right). Bars, 50 μm. **B** Bar graphs indicating % positive stained cells for indicated proteins. **C, D** Relative cell viability following PDGFR inhibitor (**C**) and CDK4/6 inhibitor (**D**) treatment at day3. DMSO, control. \* $P < 0.05$ . Data are represented as the mean  $\pm$  SEM

and Ki-67 labeling index was 20% (Additional file 1: Fig. S4A). We found the *IDH2*<sup>R172K</sup> and *TP53*<sup>R248W</sup> heterozygous SNVs in the xenografts, retained from the patient tumors (Fig. 4C). Methylation classifier analysis (11b4) indicated classification matched to diffuse glioma, IDH mutant (calibrated score 0.91); subclass high grade astrocytoma (score 0.68, Fig. 4D, Additional file 2: Table S4), mirroring the parent tumor specimen. Consistent with YMG25R parent tumor cells, gain of *PDGFRA* and amplification of *CDK4* and *MDM2* were observed, while *CDKN2A* HD was identified in the xenografts, qualifying for astrocytoma, IDH-mutant, CNS WHO grade 4 according to the WHO CNS5 criteria (Fig. 4E, Additional file 1: Fig. S4B). In addition, similar to YMG25R parent tumor (Fig. 3A–B), YMG25R xenograft cells highly expressed phospho-PDGFRα, -AKT, and -ERK as well as CDK4 and MDM2, and phospho-Rb, as compared to sham control (Fig. 4F, Additional file 1: Fig. S4C–D).

To verify if *IDH1/2*-mutant astrocytomas with *CDKN2A*, *PDGFRA*, *CDK4*, or *MDM2* CNA promotes poor prognosis, we used the GLASS and MSK diffuse glioma datasets (total 1,448 cases) [6, 19]. In these datasets, we found only one case of *IDH2*-mutant and 1p/19q non-codel tumor, but CNA was not analyzed in this case. In *IDH1*-mutant astrocytoma cases with available clinical and CNA data (total 161 cases), we found that tumors harboring either *CDKN2A* deletion, *PDGFRA* amplification, *CDK4* amplification, or *MDM2* amplification conferred poor prognosis in these cohorts (Additional file 1: Fig. S5A–B).

## Discussion

In this report, we demonstrate the first novel *IDH2*-mutant patient-derived xenograft model established from a progressed recurrent astrocytoma, *IDH2*<sup>R172K</sup> mutant, CNS WHO grade 3. Although the recurrent tumor was clinically aggressive and lethal, acquired pathogenic SNV was not annotated. Notably, we found that xenografts only formed from the recurrent tumor harboring the gain of *PDGFRA* and amplification of *CDK4* and *MDM2*, which were not identified in the initial tumor. We also found highly expressed phospho-PDGFRα and phospho-Rb in the recurrent tumor. Importantly, we confirmed that *PDGFRA*, *CDK4*, and *MDM2* CNAs as well

as *IDH2*<sup>R172K</sup> and *TP53*<sup>R248W</sup> SNVs were recapitulated in the xenograft model. On the other hand, hemizygous deletion of *CDKN2A/B* observed in both initial and recurrent parent tumors was changed to HD in the xenograft model. These findings suggest that, similar to *IDH1*-mutant astrocytoma, co-existing CNAs that activate retinoblastoma (RB) and PDGFR signaling pathway may critically drive tumor progression and xenograft formation in *IDH2*-mutant astrocytoma.

In the GLASS and MSK diffuse glioma datasets, we found only one *IDH2*-mutant astrocytic tumor in the entire cohort [6, 19]. In addition, all 4 *IDH2*-mutant and 1p/19q non-codel tumors were histologically diagnosed as WHO grade 2 and did not show putative driver SNV, except *TP53* and *ATRX* mutations in the TCGA LGG cohort [9]. On the other hand, the present case harbored *IDH2*<sup>R172K</sup> and *TP53*<sup>R248W</sup> heterozygous mutation and the DNA methylation array indicated methylation class family glioma, IDH mutant, subclass astrocytoma in primary tumor and high-grade astrocytoma in recurrent tumor. Thus, this case is particularly unique and useful for better understanding molecular mechanisms of tumor progression in *IDH2*-mutant astrocytoma.

In *IDH*-mutant astrocytoma, total CNA level was associated with poor prognosis [3, 26]. One of the most critical CNAs that drive tumor progression is *CDKN2A/B* loss. In normal cells, cell cycle regulation is critical for homeostasis. *CDKN2A* encodes p14ARF and p16INK4a, while *CDKN2B* encodes p15INK4b tumor suppressor proteins. In unstressed conditions, p16INK4a and p15INK4b bind to CDK4/CDK6, while p14ARF negatively regulates MDM2, which blocks p53 accumulation. These tumor suppressor proteins block cell cycle transition from G1 phase to S phase and induce cell cycle arrest [15]. Conversely, *CDKN2A/B* deletion inactivates p16INK4a, p14ARF, and p15INK4b, deregulates cell cycle and increases cell proliferation [36]. *CDKN2A/B* HD has been demonstrated to be strongly associated with poor prognosis in *IDH*-mutant astrocytomas [37], and the WHO CNS5 defines *IDH*-mutant astrocytomas with *CDKN2A/B* HD as CNS WHO grade 4, regardless of histological findings [8, 15, 22]. In addition to *CDKN2A* HD, recent studies indicated that *CDKN2A* hemizygous deletion also confers worse prognosis in

(See figure on next page.)

**Fig. 4** *IDH2*-mutant astrocytoma xenograft model. **A** Hematoxylin and eosin staining of non-xenograft formed mouse brain (YMG25P, upper) and xenograft formed mouse brain (YMG25R, lower). Inset, high magnification. **B** Kaplan–Meier curve estimates of mice implanted with xenograft non-forming YMG25P (blue) and forming YMG25R (red). **C** Sanger sequencing indicating *IDH2* (c.515G > A, R172K) and *TP53* (c.742C > T, R248W) mutation in YMG25R xenograft. **D** Unsupervised clustering using t-SNE analysis for YMG25R xenograft. Brain tumor classifier was determined by v11b4. **E** Copy number profiling of YMG25R xenograft. **F** Immunohistochemistry for indicated proteins in YMG25R xenograft (upper) and sham mouse brain (lower). Bars, 50 μm

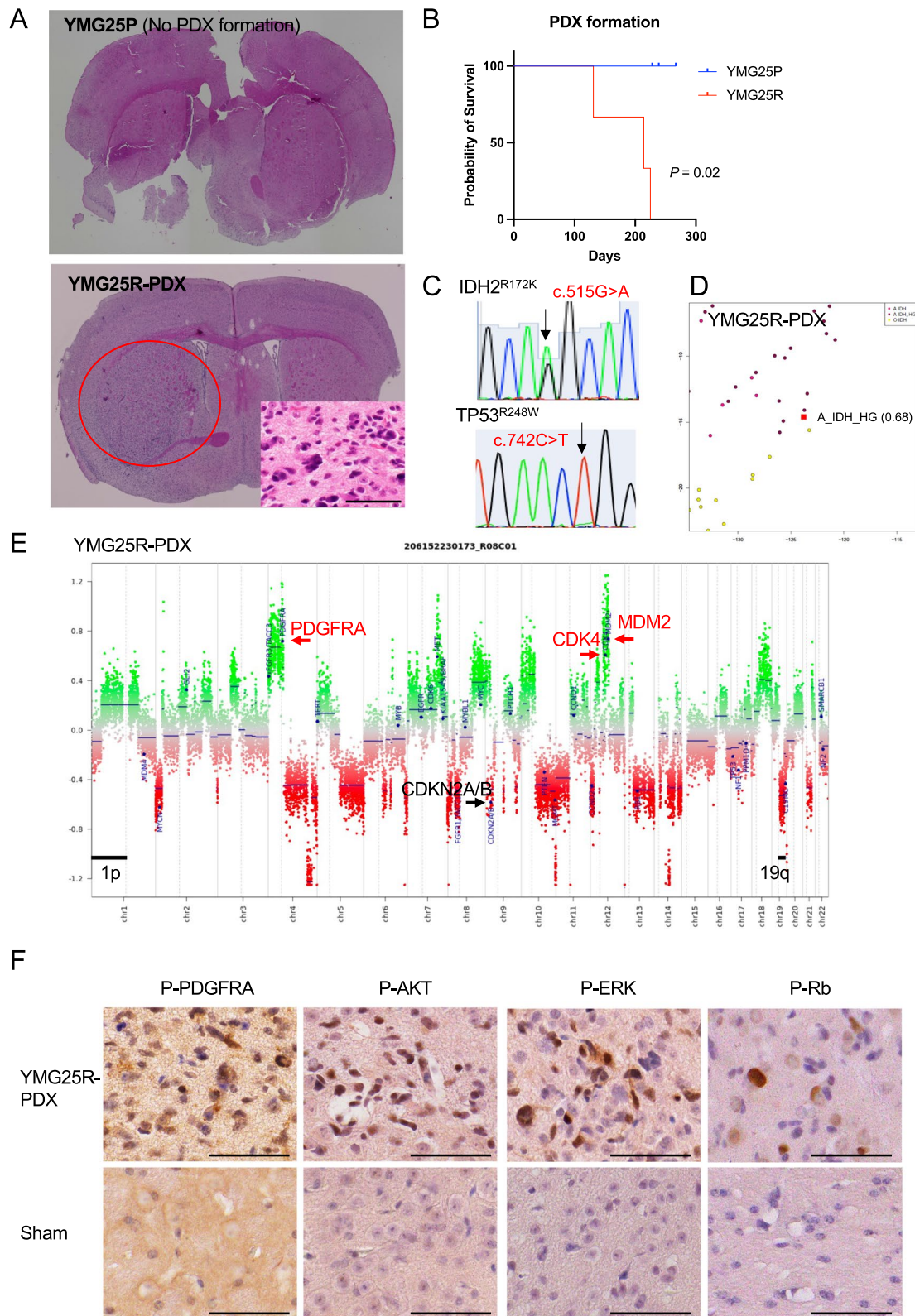


**Fig. 4** (See legend on previous page.)

*IDH*-mutant astrocytoma [18, 21]. In the present case, both initial (YMG25P) and recurrent (YMG25R) tumors were diagnosed as WHO grade 3, because of the lack of histopathological grade 4 features (i.e., necrosis and/or microvascular proliferation) and *CDKN2A/B* HD. Notably, we found *CDKN2A/B* HD in the xenograft model (YMG25R-PDX), which was only derived from the recurrent tumor. This implies that most malignant subclonal population with *CDKN2A/B* HD may have selectively generated the xenografts. However, verifying this hypothesis will require an assay system that, unlike MLPA, enables distinguishing subclonal HD from hemizygous deletion. Besides, we found *CDK4* and *MDM2* amplifications with upregulated phospho-Rb in the recurrent tumor and its xenografts, suggesting the multiple deregulated cell cycle mechanisms to support tumor progression and facilitate xenograft formation in the present case.

Although the overall prognostic significance is still controversial [37], a large-scale study demonstrated that in addition to *CDKN2A/B* deletion, *CDK4* amplification, which also deregulates Rb pathway, was associated with poor prognosis in *IDH*-mutant astrocytoma [3, 27]. Another study demonstrated that combination of *CDK4* amplification and/or *CDKN2A* deletion, and chromosome 14 loss conferred poor prognosis in astrocytoma, *IDH*-mutant [10, 11]. Moreover, co-amplification of *CDK4* and *MDM2*, which are located at the breakpoint-enriched region of chromosome 12q14-15, have been previously correlated with worse clinical prognosis in GBM [49]. In the present case, co-copy number amplification of *CDK4* and *MDM2* may have cooperatively upregulated cell cycle and promoted tumor progression. In other words, analogous to *CDKN2A/B* HD, *CDK4* and *MDM2* co-amplification might accelerate tumor progression and may induce a malignant phenotype. Of note, we found that *CDK4/6* inhibitor selectively suppressed cell viability of phospho-Rb-upregulated, recurrent cells, further supporting the critical role of cell cycle deregulation in progression in *IDH2*-mutant astrocytoma.

We also found *PDGFRA* CNA in the recurrent tumor as well as the xenograft model and upregulated protein expressions in the PI3K/AKT/mTOR pathway and RAS/RAF/MEK/ERK pathway in the recurrent tumor. It has been demonstrated that *PDGFRA* amplification is correlated with *IDH1* mutation and associated with poorer prognosis in *IDH1*-mutant astrocytomas, CNS WHO grade 4, as compared to those without *PDGFRA* amplification [32]. Yang et al. stratified *IDH*-mutant lower-grade astrocytomas by the presence of *CDKN2A* HD, *CDK4* amplification, and *PDGFRA* amplification. These copy number alterations were found in a mutually exclusive manner [47], unlike the present case. They found that

tumors with *PDGFRA* amplification (high risk group) had poorer prognosis than those with *CDKN2A* homozygous deletion or *CDK4* amplification (intermediate group) and copy number non-altered group (low risk group) [47]. *PDGFRA* is a member of the receptor tyrosine kinase family and is involved in stimulating the PI3K/AKT/mTOR pathway and RAS/RAF/MEK/ERK pathway [7]. *PDGFRA* plays a role in normal gliogenesis of the central nervous system and *PDGFRA* high-level amplification and gain has been associated with high grade malignancy in gliomas [1, 34]. In an experimental model, PDGFA enhanced the growth of *IDH1*<sup>R132H</sup> mutant immortal *Cdkn2a*, *Atrx*, and *Pten* deficient astrocytes and PDGFA cooperated with *IDH1*<sup>R132H</sup> and loss of *Cdkn2a*, *Atrx*, and *Pten* to promote glioma formation in vivo [31]. Another study using the RCAS/TVA system demonstrated that glioma-genesis in the context of mutant *IDH1* with *shp53* and/or *Cdkn2a* loss, was only facilitated when combined with PDGFa [2]. Importantly, the present data demonstrated that PDGFR inhibitor potently suppressed cell viability in recurrent tumor cells with *PDGFRA* gain, whereas there was no difference after PI3K inhibitor treatment. These clinical and preclinical findings support the role of *PDGFRA* gene alterations and downstream multiple signaling pathways, including PI3K/AKT/mTOR pathway and RAS/RAF/MEK/ERK pathway, in promoting progression of not only *IDH1*-mutant, but also *IDH2*-mutant astrocytoma.

Although a recent clinical trial reported that an inhibitor targeting mutant *IDH1* and *IDH2* induced durable therapeutic efficacy in lowgrade glioma [24], the impact of directly targeting mutant *IDH* for high-grade glioma is under clinical investigation. In accord with our previous study that *IDH1* inhibitor was not sufficient to induce anti-tumor effects in *IDH1*-mutant high-grade gliomas [40], we did not find decreased cell viability nor histone methylation status changes after mutation specific *IDH2* inhibitor treatment of recurrent cells. However, as the drug exposure was short-term, further study is needed to address if prolonged use of mutant specific *IDH2* inhibitor can induce anti-tumor effects in *IDH2* mutant high-grade astrocytoma. Impact of *IDH2* inhibitors on earlier stages of tumorigenesis also requires future investigations.

Altogether, this study demonstrated the pivotal biological role of gene alterations that activate RB pathway and PDGFR pathway in the progression of *IDH2*-mutant astrocytoma. This molecular mechanism in disease progression seems analogous to *IDH1*-mutant astrocytoma. We also established the first *IDH2*-mutant astrocytoma xenograft model derived from progressed disease. Together with the clinical

characteristics and xenograft model, we found that CNAs involving RB pathway and *PDGFRA* promote tumor progression in astrocytoma, IDH2-mutant.

## Supplementary Information

The online version contains supplementary material available at <https://doi.org/10.1186/s40478-023-01683-x>.

**Additional file 1. Figure S1. A** Positron emission tomography indicated uptake (arrow head) of 18F-FDG (left) and 11C-methionine (right) in initial tumor (YMG25P). **B** Immunohistochemistry for indicated proteins in YMG25P and YMG25R tumor. Bars, 50µm; **Figure S2. A** Multiplex ligation-dependent probe amplification (MLPA) indicating copy number alterations for indicated genes in YMG25P (upper) and YMG25R (lower). **B** MLPA indicating chromosome partial deletion of 19q, CDKN2A hemizygous loss, and IDH2R172K mutation in YMG25P (upper). MLPA indicating chromosome partial deletion of 1p and 19q, CDKN2A hemizygous loss, and IDH2R172K mutation in YMG25R (lower). **C** DNA methylation array indicating MGMT promotor methylation status in initial tumor (YMG25P, left) and recurrent tumor (YMG25R, right); **Figure S3. A** Immunohistochemistry for indicated proteins in initial (YMG25P, upper) and recurrent tumors (YMG25R, lower). **B** Western blotting of indicated proteins in YMG25P and YMG25R tumors. Bars, 50µm. **C** Relative cell viability of PI3K inhibitor (LY294002) and AKT inhibitor (GDC-0068) at day3. **D** Relative cell viability of YMG25R cells after IDH2 inhibitor (AG-221) at day 9. DMSO, control. Data are represented as the mean ± SEM. **E, F** Western blotting of indicated proteins in YMG25R cells after DMSO or AG-221 (5µM) treatment for 12 days. NS, not significant; **Figure S4. A** Immunohistochemistry for indicated proteins in YMG25R xenograft tumor. **B** Multiplex ligation-dependent probe amplification indicating copy number alterations for indicated genes in YMG25R xenograft. **C** Immunohistochemistry for indicated proteins in YMG25R xenograft (upper) and sham mouse brain (lower). Bars, 50µm. **D** Bar graphs indicating % immuno-positive cells for indicated proteins. \**P* < 0.05; **Figure S5. A** Genomic landscape of IDH1-mutant astrocytoma with/without copy number alterations. GLASS and MSK lower-grade glioma cohorts are merged for analysis. **B** Kaplan-Meier curve showing survival difference of IDH1-mutant astrocytoma with/without either *PDGFRA* amplification, *CDK4* amplification, *MDM2* amplification, or *CDKN2A* deletion. *P*-value is determined by Log-rank test.

**Additional file 2. Table S1.** Primers used for PCR amplification and sequencing; **Table S2.** Whole exome sequencing for initial tumor (YMG25P); **Table S3.** Whole exome sequencing for recurrent tumor (YMG25R); **Table S4.** DNA methylation array-based tumor classification (version 11b4); **Table S5:** DNA methylation array-based tumor classification (version 12.8).

## Acknowledgements

The authors thank Dr. Koichi Ichimura and Mrs. Emi Hirata and Yuko Matsushita for technical and administrative assistance. This work was supported by Grant-Aid for Scientific Research (19K09488 and 22K09210 to KT), Strategic Research Promotion of Yokohama City University Research, Yokohama Foundation for Advancement of Medical Science (to KT).

## Author contributions

KT led the study, collected samples, designed experiments, performed experiments, interpreted data, and wrote the manuscript. YM, TN, and TY provided tumor samples and associated clinical details. TH, AO, HHO, HHa, KyS, and MK performed experiments. HI, KaS, SF, and TK performed the histological classification of tumor samples. DPC and HW designed experiments and supervised of this study. All authors read and approved the final manuscript.

## Funding

This work was supported by Grant-Aid for Scientific Research (19K09488 and 22K09210 to KT), Strategic Research Promotion of Yokohama City University Research, Yokohama Foundation for Advancement of Medical Science (to KT).

## Availability of data and materials

The genomic and epigenomic information used in this study was deposited in the National Bioscience Database Center under accession number JSUB000906. The data generated in this study are available within the article and the online supplementary material.

## Declarations

### Ethical approval

This study was conducted in accordance with the Declaration of Helsinki and approved by the Institutional Review Board of Yokohama City University (YCU, Yokohama, Japan, A171130006 and B190700012).

### Consent for publication

Written informed consent was obtained from the patient and his family. All authors consented to publication.

### Competing interests

The authors declare that they have no competing conflict of interest.

Received: 18 August 2023 Accepted: 2 November 2023

Published online: 27 November 2023

## References

- Alentorn A, Marie Y, Carpentier C, Boisselier B, Giry M, Labussiere M, Mokhtari K, Hoang-Xuan K, Sanson M, Delattre JY et al (2012) Prevalence, clinico-pathological value, and co-occurrence of *PDGFRA* abnormalities in diffuse gliomas. *Neuro Oncol* 14:1393–1403. <https://doi.org/10.1093/neuonc/nos217>
- Amankulor NM, Kim Y, Arora S, Kargl J, Szulzewsky F, Hanke M, Margineantu DH, Rao A, Bolouri H, Delrow J et al (2017) Mutant IDH1 regulates the tumor-associated immune system in gliomas. *Genes Dev* 31:774–786. <https://doi.org/10.1101/gad.294991.116>
- Aoki K, Nakamura H, Suzuki H, Matsuo K, Kataoka K, Shimamura T, Motomura K, Ohka F, Shiina S, Yamamoto T et al (2018) Prognostic relevance of genetic alterations in diffuse lower-grade gliomas. *Neuro Oncol* 20:66–77. <https://doi.org/10.1093/neuonc/nox132>
- Arita H, Narita Y, Fukushima S, Tateishi K, Matsushita Y, Yoshida A, Miyakita Y, Ohno M, Collins VP, Kawahara N et al (2013) Upregulating mutations in the TERT promoter commonly occur in adult malignant gliomas and are strongly associated with total 1p19q loss. *Acta Neuropathol* 126:267–276. <https://doi.org/10.1007/s00401-013-1141-6>
- Bai H, Harmanci AS, Erson-Omay EZ, Li J, Coskun S, Simon M, Krischek B, Ozduman K, Omay SB, Sorensen EA et al (2016) Integrated genomic characterization of IDH1-mutant glioma malignant progression. *Nat Genet* 48:59–66. <https://doi.org/10.1038/ng.3457>
- Barthel FP, Johnson KC, Varn FS, Moskalik AD, Tanner G, Kocakavuk E, Anderson KJ, Abiola O, Aldape K, Alfaro KD et al (2019) Longitudinal molecular trajectories of diffuse glioma in adults. *Nature* 576:112–120. <https://doi.org/10.1038/s41586-019-1775-1>
- Blume-Jensen P, Hunter T (2001) Oncogenic kinase signalling. *Nature* 411:355–365. <https://doi.org/10.1038/35077225>
- Brat DJ, Aldape K, Colman H, Figarella-Branger D, Fuller GN, Giannini C, Holland EC, Jenkins RB, Kleinschmidt-DeMasters B, Komori T et al (2020) CIMPACT-NOW update 5: recommended grading criteria and terminologies for IDH-mutant astrocytomas. *Acta Neuropathol* 139:603–608. <https://doi.org/10.1007/s00401-020-02127-9>
- Cancer Genome Atlas Research N, Brat DJ, Verhaak RG, Aldape KD, Yung WK, Salama SR, Cooper LA, Rheinbay E, Miller CR, Vitucci M et al (2015) Comprehensive, integrative genomic analysis of diffuse lower-grade gliomas. *N Engl J Med* 372:2481–2498. <https://doi.org/10.1056/NEJMoA1402121>
- Cimino PJ, Holland EC (2019) Targeted copy number analysis outperforms histologic grading in predicting patient survival for WHO grades II/III IDH-mutant astrocytomas. *Neuro Oncol* 21:819–821. <https://doi.org/10.1093/neuonc/noz052>

11. Cimino PJ, Zager M, McFerrin L, Wirsching HG, Bolouri H, Hentschel B, von Deimling A, Jones D, Reifenberger G, Weller M et al (2017) Multidimensional scaling of diffuse gliomas: application to the 2016 World Health Organization classification system with prognostically relevant molecular subtype discovery. *Acta Neuropathol Commun* 5:39. <https://doi.org/10.1186/s40478-017-0443-7>
12. Dang L, White DW, Gross S, Bennett BD, Bittinger MA, Driggers EM, Fantin VR, Jang HG, Jin S, Keenan MC et al (2009) Cancer-associated IDH1 mutations produce 2-hydroxyglutarate. *Nature* 462:739–744. <https://doi.org/10.1038/nature08617>
13. DiNardo CD, Schuh AC, Stein EM, Montesinos P, Wei AH, de Botton S, Zeidan AM, Fathi AT, Kantarjian HM, Bennett JM et al (2021) Enasidenib plus azacitidine versus azacitidine alone in patients with newly diagnosed, mutant-IDH2 acute myeloid leukaemia (AG221-AML-005): a single-arm, phase 1b and randomised, phase 2 trial. *Lancet Oncol* 22:1597–1608. [https://doi.org/10.1016/S1470-2045\(21\)00494-0](https://doi.org/10.1016/S1470-2045(21)00494-0)
14. Figueroa ME, Abdel-Wahab O, Lu C, Ward PS, Patel J, Shih A, Li Y, Bhagwat N, Vasanthakumar A, Fernandez HF et al (2010) Leukemic IDH1 and IDH2 mutations result in a hypermethylation phenotype, disrupt TET2 function, and impair hematopoietic differentiation. *Cancer Cell* 18:553–567. <https://doi.org/10.1016/j.ccr.2010.11.015>
15. Fortin Ensign SP, Jenkins RB, Giannini C, Sarkaria JN, Galanis E, Kizilbash SH (2023) Translational significance of CDKN2A/B homozygous deletion in isocitrate dehydrogenase-mutant astrocytoma. *Neuro Oncol* 25:28–36. <https://doi.org/10.1093/neuonc/noac205>
16. Fujimoto K, Arita H, Satomi K, Yamasaki K, Matsushita Y, Nakamura T, Miyakita Y, Umehara T, Kobayashi K, Tamura K et al (2021) TERT promoter mutation status is necessary and sufficient to diagnose IDH-wildtype diffuse astrocytic glioma with molecular features of glioblastoma. *Acta Neuropathol* 142:323–338. <https://doi.org/10.1007/s00401-021-02337-9>
17. Hayashi T, Tateishi K, Matsuyama S, Iwashita H, Miyake Y, Oshima A, Homma H, Sasame J, Takabayashi K, Sugino K et al (2023) Intraoperative integrated diagnostic system for malignant central nervous system tumors. *Clin Cancer Res*. <https://doi.org/10.1158/1078-0432.CCR-23-1660>
18. Hickman RA, Gedvilaite E, Ptashkin R, Reiner AS, Cimera R, Nandakumar S, Price A, Vanderbilt C, Fahy T, Young RJ et al (2023) CDKN2A/B mutations and allele-specific alterations stratify survival outcomes in IDH-mutant astrocytomas. *Acta Neuropathol*. <https://doi.org/10.1007/s00401-023-02639-0>
19. Jonsson P, Lin AL, Young RJ, DiStefano NM, Hyman DM, Li BT, Berger MF, Zehir A, Ladanyi M, Solit DB et al (2019) Genomic correlates of disease progression and treatment response in prospectively characterized gliomas. *Clin Cancer Res* 25:5537–5547. <https://doi.org/10.1158/1078-0432.CCR-19-0032>
20. Killela PJ, Reitman ZJ, Jiao Y, Bettegowda C, Agrawal N, Diaz LA Jr, Friedman AH, Friedman H, Gallia GL, Giovannella BC et al (2013) TERT promoter mutations occur frequently in gliomas and a subset of tumors derived from cells with low rates of self-renewal. *Proc Natl Acad Sci U S A* 110:6021–6026. <https://doi.org/10.1073/pnas.1303607110>
21. Kocakavuk E, Johnson KC, Sabedot TS, Reinhardt HC, Noushmehr H, Verhaak RGW (2023) Hemizygous CDKN2A deletion confers worse survival outcomes in IDHmut-noncode gliomas. *Neuro Oncol* 25:1721–1723. <https://doi.org/10.1093/neuonc/noad095>
22. Louis DN, Perry A, Wesseling P, Brat DJ, Cree IA, Figarella-Branger D, Hawkins C, Ng HK, Pfister SM, Reifenberger G et al (2021) The 2021 WHO classification of tumors of the central nervous system: a summary. *Neuro Oncol* 23:1231–1251. <https://doi.org/10.1093/neuonc/noab106>
23. Ma P, Fu Y, Cai MC, Yan Y, Jing Y, Zhang S, Chen M, Wu J, Shen Y, Zhu L et al (2017) Simultaneous evolutionary expansion and constraint of genomic heterogeneity in multifocal lung cancer. *Nat Commun* 8:823. <https://doi.org/10.1038/s41467-017-00963-0>
24. Mellinghoff IK, van den Bent MJ, Blumenthal DT, Touat M, Peters KB, Clarke J, Mendez J, Yust-Katz S, Welsh L, Mason WP et al (2023) Vorasidenib in IDH1- or IDH2-mutant low-grade glioma. *N Engl J Med*. <https://doi.org/10.1056/NEJMoa2304194>
25. Miller JJ, Gonzalez Castro LN, McBrayer S, Weller M, Cloughesy T, Portnow J, Andronesi O, Barnholtz-Sloan JS, Baumert BG, Berger MS et al (2022) Isocitrate dehydrogenase (IDH) mutant gliomas: a Society for Neuro-Oncology (SNO) consensus review on diagnosis, management, and future directions. *Neuro Oncol*. <https://doi.org/10.1093/neuonc/noac207>
26. Mirchia K, Sathe AA, Walker JM, Fudym Y, Galbraith K, Viapiano MS, Corona RJ, Snuderl M, Xing C, Hatanpaa KJ et al (2019) Total copy number variation as a prognostic factor in adult astrocytoma subtypes. *Acta Neuropathol Commun* 7:92. <https://doi.org/10.1186/s40478-019-0746-y>
27. Mirchia K, Snuderl M, Galbraith K, Hatanpaa KJ, Walker JM, Richardson TE (2019) Establishing a prognostic threshold for total copy number variation within adult IDH-mutant grade II/III astrocytomas. *Acta Neuropathol Commun* 7:121. <https://doi.org/10.1186/s40478-019-0778-3>
28. Miyake Y, Fujii K, Nakamura T, Ikegaya N, Matsushita Y, Gobayashi Y, Iwashita H, Udaka N, Kumagai J, Murata H et al (2021) IDH-mutant astrocytoma with chromosome 19q13 deletion manifesting as an oligodendroglioma-like morphology. *J Neuropathol Exp Neurol* 80:247–253. <https://doi.org/10.1093/jnen/nlaa161>
29. Noushmehr H, Weisenberger DJ, Diefes K, Phillips HS, Pujara K, Berman BP, Pan F, Pelloski CE, Sulman EP, Bhat KP et al (2010) Identification of a CpG island methylator phenotype that defines a distinct subgroup of glioma. *Cancer Cell* 17:510–522. <https://doi.org/10.1016/j.ccr.2010.03.017>
30. Parsons DW, Jones S, Zhang X, Lin JC, Leary RJ, Angenendt P, Mankoo P, Carter H, Siu IM, Gallia GL et al (2008) An integrated genomic analysis of human glioblastoma multiforme. *Science* 321:1807–1812. <https://doi.org/10.1126/science.1164382>
31. Philip B, Yu DX, Silvis MR, Shin CH, Robinson JP, Robinson GL, Welker AE, Angel SN, Tripp SR, Sonnen JA et al (2018) Mutant IDH1 promotes glioma formation in vivo. *Cell Rep* 23:1553–1564. <https://doi.org/10.1016/j.celrep.2018.03.133>
32. Phillips JJ, Aranda D, Ellison DW, Judkins AR, Croul SE, Brat DJ, Ligon KL, Horbinski C, Venneti S, Zadeh G et al (2013) PDGFRA amplification is common in pediatric and adult high-grade astrocytomas and identifies a poor prognostic group in IDH1 mutant glioblastoma. *Brain Pathol* 23:565–573. <https://doi.org/10.1111/bpa.12043>
33. Richardson TE, Snuderl M, Serrano J, Karajannis MA, Heguy A, Oliver D, Raisanen JM, Maher EA, Pan E, Barnett S et al (2017) Rapid progression to glioblastoma in a subset of IDH-mutated astrocytomas: a genome-wide analysis. *J Neurooncol*. <https://doi.org/10.1007/s11060-017-2431-y>
34. Richardson WD, Pringle N, Mosley MJ, Westermarck B, Dubois-Dalcq M (1988) A role for platelet-derived growth factor in normal gliogenesis in the central nervous system. *Cell* 53:309–319. [https://doi.org/10.1016/0092-8674\(88\)90392-3](https://doi.org/10.1016/0092-8674(88)90392-3)
35. Sanson M, Marie Y, Paris S, Idbaih A, Laffaire J, Ducray F, El Hallani S, Boisselier B, Mokhtari K, Hoang-Xuan K et al (2009) Isocitrate dehydrogenase 1 codon 132 mutation is an important prognostic biomarker in gliomas. *J Clin Oncol* 27:4150–4154. <https://doi.org/10.1200/JCO.2009.21.9832>
36. Sharpless NE (2005) INK4a/ARF: a multifunctional tumor suppressor locus. *Mutat Res* 576:22–38. <https://doi.org/10.1016/j.mrfmmm.2004.08.021>
37. Shirahata M, Ono T, Stichel D, Schrimpf D, Reuss DE, Sahm F, Koelsche C, Wefers A, Reinhardt A, Huang K et al (2018) Novel, improved grading system(s) for IDH-mutant astrocytic gliomas. *Acta Neuropathol* 136:153–166. <https://doi.org/10.1007/s00401-018-1849-4>
38. Tateishi K, Miyake Y, Kawazu M, Sasaki N, Nakamura T, Sasame J, Yoshii Y, Ueno T, Miyake A, Watanabe J et al (2020) A hyperactive RelA/p65-hexokinase 2 signaling axis drives primary central nervous system lymphoma. *Cancer Res* 80:5330–5343. <https://doi.org/10.1158/0008-5472.CAN-20-2425>
39. Tateishi K, Nakamura T, Juratli TA, Williams EA, Matsushita Y, Miyake S, Nishi M, Miller JJ, Tummala SS, Fink AL et al (2019) PI3K/AKT/mTOR pathway alterations promote malignant progression and xenograft formation in oligodendroglial tumors. *Clin Cancer Res* 25:4375–4387. <https://doi.org/10.1158/1078-0432.CCR-18-4144>
40. Tateishi K, Wakimoto H, Iafra AJ, Tanaka S, Loebel F, Lelic N, Wiederschain D, Bedel O, Deng G, Zhang B et al (2015) Extreme vulnerability of IDH1 mutant cancers to NAD+ depletion. *Cancer Cell* 28:773–784. <https://doi.org/10.1016/j.ccell.2015.11.006>
41. Wakimoto H, Kesari S, Farrell CJ, Curry WT Jr, Zaupa C, Aghi M, Kuroda T, Stemmer-Rachamimov A, Shah K, Liu TC et al (2009) Human glioblastoma-derived cancer stem cells: establishment of invasive glioma models and treatment with oncolytic herpes simplex virus vectors. *Cancer Res* 69:3472–3481. <https://doi.org/10.1158/0008-5472.CAN-08-3886>
42. Wakimoto H, Tanaka S, Curry WT, Loebel F, Zhao D, Tateishi K, Chen J, Kofas LK, Lelic N, Kim JC et al (2014) Targetable signaling pathway mutations are associated with malignant phenotype in IDH-mutant gliomas.

- Clin Cancer Res 20:2898–2909. <https://doi.org/10.1158/1078-0432.CCR-13-3052>
43. Wang F, Travins J, DeLaBarre B, Penard-Lacronique V, Schalm S, Hansen E, Straley K, Kernysky A, Liu W, Gliser C et al (2013) Targeted inhibition of mutant IDH2 in leukemia cells induces cellular differentiation. *Science* 340:622–626. <https://doi.org/10.1126/science.1234769>
  44. Wang HY, Tang K, Liang TY, Zhang WZ, Li JY, Wang W, Hu HM, Li MY, Wang HQ, He XZ et al (2016) The comparison of clinical and biological characteristics between IDH1 and IDH2 mutations in gliomas. *J Exp Clin Cancer Res* 35:86. <https://doi.org/10.1186/s13046-016-0362-7>
  45. Ward PS, Patel J, Wise DR, Abdel-Wahab O, Bennett BD, Collier HA, Cross JR, Fantin VR, Hedvat CV, Perl AE et al (2010) The common feature of leukemia-associated IDH1 and IDH2 mutations is a neomorphic enzyme activity converting alpha-ketoglutarate to 2-hydroxyglutarate. *Cancer Cell* 17:225–234. <https://doi.org/10.1016/j.ccr.2010.01.020>
  46. Yan H, Parsons DW, Jin G, McLendon R, Rasheed BA, Yuan W, Kos I, Batinic-Haberle I, Jones S, Riggins GJ et al (2009) IDH1 and IDH2 mutations in gliomas. *N Engl J Med* 360:765–773. <https://doi.org/10.1056/NEJMoa0808710>
  47. Yang RR, Shi ZF, Zhang ZY, Chan AK, Aibaidula A, Wang WW, Kwan JSH, Poon WS, Chen H, Li WC et al (2020) IDH mutant lower grade (WHO Grades II/III) astrocytomas can be stratified for risk by CDKN2A, CDK4 and PDGFRA copy number alterations. *Brain Pathol* 30:541–553. <https://doi.org/10.1111/bpa.12801>
  48. Yen K, Travins J, Wang F, David MD, Artin E, Straley K, Padyana A, Gross S, DeLaBarre B, Tobin E et al (2017) AG-221, a first-in-class therapy targeting acute myeloid leukemia harboring oncogenic IDH2 mutations. *Cancer Discov* 7:478–493. <https://doi.org/10.1158/2159-8290.CD-16-1034>
  49. Zheng S, Fu J, Vegesna R, Mao Y, Heathcock LE, Torres-Garcia W, Ezhilarasan R, Wang S, McKenna A, Chin L et al (2013) A survey of intragenic breakpoints in glioblastoma identifies a distinct subset associated with poor survival. *Genes Dev* 27:1462–1472. <https://doi.org/10.1101/gad.213686.113>

## Publisher's Note

Springer Nature remains neutral with regard to jurisdictional claims in published maps and institutional affiliations.

Ready to submit your research? Choose BMC and benefit from:

- fast, convenient online submission
- thorough peer review by experienced researchers in your field
- rapid publication on acceptance
- support for research data, including large and complex data types
- gold Open Access which fosters wider collaboration and increased citations
- maximum visibility for your research: over 100M website views per year

At BMC, research is always in progress.

Learn more [biomedcentral.com/submissions](https://biomedcentral.com/submissions)

